Photochemical & Photobiological Sciences

ROYAL SOCIETY OF CHEMISTRY

PAPER

Cite this: *Photochem. Photobiol. Sci.*, 2020, **19**, 1280

Electronic interactions between a quaternary pyridyl-β-diketonate and anionic clay nanosheets facilitate intense photoluminescence†

Tomohiko Okada, *[a,b] Yoko Miyamoto,[b] Haruka Kurihara,[b] Yoshifumi Mochiduki,[c] Shiho Katsumi[c] and Fuyuki Ito[c]

Received 26th April 2020,
Accepted 19th July 2020

DOI: 10.1039/d0pp00166j

rsc.li/pps

Electrostatic interactions between a quaternary pyridyl-β-diketonate and anionic charged nanosheets were observed to produce a highly emissive dispersion in a rich water solution. A greater fluorescence quantum yield of approximately 50% was obtained when a luminogenic β-diketonate, 1-(4-methoxyphenyl)-3-(3-hydroxyethyl-pyridinium bromide)-1,3-propandione (prepared by the Claisen condensation reaction and subsequent quaternization), was molecularly dispersed and enclosed by a couple of atomically flat ultrathin (approximately 1.0 nm) silicate sheets of anionic layered clay. By accommodating β-diketonate into a narrow interlamellar space (approximately 0.4 nm distance), the molecular motion was suppressed, as confirmed by a smaller non-radiative relaxation rate constant, which was obtained by time-resolved luminescence and quantum yield measurements. Because the dense packing of β-diketonate quenched the excited state, the isolation of luminogens by the co-adsorption of photochemical inert cations (tetramethylammonium and benzylammonium) was prevented by concentration quenching. A lower quantum yield was obtained by expanding the interlayer distance above 1.0 nm by co-adsorbing a photo-inactive water-soluble polymer, poly(vinylpyrrolidone). Therefore, the fixation and spatial separation of β-diketonate in the narrow interlayer space was determined to be essential for obtaining strong emission.

1. Introduction

The development of highly emissive solids (in particular in aqueous phase and solid state) is crucial for photochemical and optical applications. Robust and stable assemblies of luminophores are required to obtain strong and efficient emission. Aggregation-induced emission (AIE: highly emissive when clustered as aggregates in poor solvents or in the solid state) is a typical example because it is based on the restriction of molecular motion in the assemblies.[1,2] Coordination to metal cations and hybridization of luminophores on solid surfaces are other methodologies to produce strong emission (fluorescence). In particular, the phenomenon occurring on solid surfaces has been recently referred to as "surface-fixation induced emission (S-FIE)".[3–5] Chemical stability against decomposition and elimination is essential to create emissive materials.

Dibenzoyl and dinaphthoyl β-diketones have been extensively studied in luminophores as part of metal–organic complexes, AIE luminogenic dyes, and hybrids with solid surfaces or matrices. Many reports on lanthanide–organic complexes have shown that these complexes are adequate ligands because β-diketonates protect lanthanide ions from vibrational coupling and increase the light absorption cross section (*i.e.*, antenna effect) owing to their Lewis basic nature, proximity, and planarity.[6,7] Through coupling with functional groups, the molecular design of β-diketonates has improved luminescence efficiency and sensitivity toward target molecules.[8–12] Boron (or difluoroboron) has been coordinated to β-diketonates as a pinning substituent to restrict intramolecular rotational motion, which resulted in good AIE characteristics.[13–22] However, the performance of hydrolysis to eliminate difluoro-

[a]*Research Initiative for Supra-Materials, Shinshu University, Nagano 380-8553, Japan. E-mail: tomohiko@shinshu-u.ac.jp*
[b]*Department of Chemistry and Material Engineering, Shinshu University, Nagano 380-8553, Japan*
[c]*Institute of Education, Shinshu University, Nagano 380-8544, Japan*

†Electronic supplementary information (ESI) available: ^{1}H NMR (Fig. S1) and MS spectra of BDKPy$^+$Br$^-$ (Fig. S2), absorption spectrum of BDKPy$^+$Br$^-$ (Fig. S3), absorption spectra of BDKPy$^+$-S0.1 in water, methanol, acetonitrile, tetrahydrofuran, and chloroform (Fig. S4), absorption spectra of BDKPy$^+$-S*n* in a water/ethanol mixture (Fig. S5), photoluminescence spectra of BDKPy$^+$Br$^-$ in water, methanol, acetonitrile, tetrahydrofuran, and chloroform and that (Fig. S7) of mixed solution (water/ethanol = 9 : 1) of BDKPy$^+$Br$^-$, and absorption spectra of BDKPy$^+$-S0.1-PVP*n* in a water/ethanol mixture (Fig. S8). See DOI: 10.1039/d0pp00166j

boron deactivates except for coupling with poly(lactic acid) in water.[13] Although fluoroboron-free β-diketonate (dinaphthoylmethane β-diketonate) itself exhibits the AIE phenomena,[21,22] luminophores, which are emissive under moderate packing, become dark in a dense face-to-face packing structure owing to aggregation-caused quenching or concentration quenching.[21]

Fluoroboron-free β-diketonates that are sensitive to chemical environments have been dispersed in lanthanide-doped sol–gel glasses,[23–25] periodic porous silica-based materials,[25] multi-walled carbon nanofibers,[26] and polymers.[25,27] The optical transparency in ultraviolet (UV) and visible light range is advantageous for evaluating the optical properties of dyes and for applying them to the fabrication of photochemical, optical, and bioimaging materials. We are interested in enhancing emission using a specific interaction with optically transparent solid surfaces for organizing β-diketones in a controlled manner (*e.g.*, location, orientation, and packing). The electrostatic interactions of negatively charged layered silicate were used to direct molecular organization.[28] Hydrothermally synthesized layered silicate (Sumecton SA, synthetic saponite, a smectite group of layered clay minerals) was used; an ultrathin (1.0 nm) crystalline silicate layer was superimposed by hydrated exchangeable cations, which compensate for the negatively charged silicate layers. Cation-exchangeable layered silicates (mainly smectites) have been intensely investigated for the organization of various cationic dyes for photochemical and optical functional hybrid applications.[29–33] Owing to strong dye-layered silicate interactions, several cationic species were tightly immobilized with the planar conformation in interlayer spaces.[4,5,34–37] The restriction of molecular motion has resulted in the appearance of strong emission even at ambient temperature (S-FIE).[3–5] In other cationic dye–silicate systems, the isolation of proximal dyes has been effective in avoiding concentration quenching by the co-insertion of photo-inactive species in interlayer spaces.[38–41]

Here, we report the enhanced emission of a cationic fluoroboron-free β-diketonate, which occurs by tight binding and molecular isolation with the aid of electrostatic dye–silicate interactions. Quaternary pyridyl-β-diketonate ($BDKPy^+Br^-$; Scheme 1) employed in this study compensates part of the permanent negative charge in layered silicate *via* cation-exchange reactions. Another part of the negative charge will be compensated by photo-inactive cations (*e.g.*, tetramethylammonium and benzylammonium) for the adjusted packing of the $BDKPy^+$ luminogen. A water-soluble polymer, poly(vinylpyrrolidone), will be forced to surround $BDKPy^+$ in close contact in sterically limited interlayer spaces; otherwise, the expansion of the interlamellar space will result in a release from tight binding by the large quantities of intercalated poly(vinylpyrrolidone). We will discuss emission efficiency in relation to the interlayer expansion of layered silicate (Sumecton SA) and the packing density of $BDKPy^+$.

2. Experimental

Reagents and materials

Sodium hydride (NaH, M_w = 24.00 g mol^{-1}, Fuji Film Wako Pure Chemical Ind., Ltd), 4′-methoxyacetophenone ($C_9H_{10}O_2$, M_w = 150.18 g mol^{-1}, Tokyo Chemical Industry Co., Ltd), ethyl isonicotinate ($C_8H_9NO_2$, M_w = 151.17 g mol^{-1}, Tokyo Chemical Industry Co., Ltd), 2-bromoethanol (C_2H_5BrO, M_w = 124.97 g mol^{-1}, Tokyo Chemical Industry Co., Ltd), sodium sulfate (Na_2SO_4, M_w = 142.04 g mol^{-1}, Fuji Film Wako Pure Chemical Ind., Ltd), ethyl acetate ($C_4H_8O_2$, M_w = 88.11 g mol^{-1}, Kanto Chemical Co. Inc.), toluene (dehydrated, Fuji Film Wako Pure Chemical Ind., Ltd), and tetrahydrofuran (THF, dehydrated, stabilizer free, Kanto Chemical Co. Inc.) were used without further purification. Layered silicate (Sumecton SA, JCSS–3501; hereafter abbreviated as SA; $(Na_{0.49}Ca_{0.14})^{0.77+}[(Mg_{5.97}Al_{0.03})(Si_{7.20}Al_{0.80})O_{20}(OH)_4]^{0.77-}$, supplied by Kunimine Ind. Co., Ltd) is a synthetic saponite, which is the reference clay sample of the Clay Science Society of Japan. The ζ potential of pristine SA is negative in the higher pH region (4 to 9), indicating that a permanent charge is dominant on the surfaces.[42] The cation-exchange capacity (CEC) of SA is 0.71 mEq g^{-1} of clay. Ethanol (99.5%), tetramethylammonium chloride (abbreviated as TMA^+Cl^-), and poly(vinylpyrrolidone) (abbreviated as PVP) were purchased from Fuji Film Wako Pure Chemical Ind., Ltd. Benzylamine hydrochloride (abbreviated as BA–HCl) was purchased from Merck Schuchardt OHG (Germany). These materials were used as received.

Synthesis of 1-(4-methoxyphenyl)-3-(3-hydroxyethyl-pyridinium bromide)-1,3-propandione ($BDKPy^+Br^-$) by Claisen condensation[43]

Sodium hydride (0.51 g, 20 mmol) was added to the solution of ethyl isonicotinate (0.61 g, 4 mmol) and 4′-methoxyacetophenone (0.15 g, 11 mmol) dissolved in dry THF (10 mL), followed by refluxing for 6 h at 339 K. After the Claisen condensation reaction, as shown in Scheme 2, the reaction was quenched by cooling to room temperature using 20 mL of a saturated $NaHCO_3$ aqueous solution; the solvent was evaporated under reduced pressure. The product dissolved in ethyl acetate was washed with brine and dried over anhydrous sodium sulfate. After the insoluble fraction in the organic phase was separated by filtration, crystallization from the

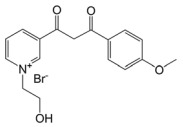

Scheme 1 Molecular structure of $BDKPy^+Br^-$.

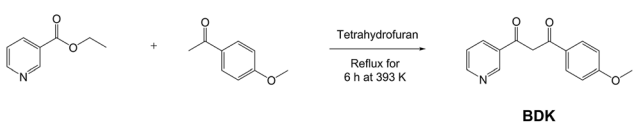

Scheme 2 Synthesis of BDK *via* the Claisen condensation reaction.

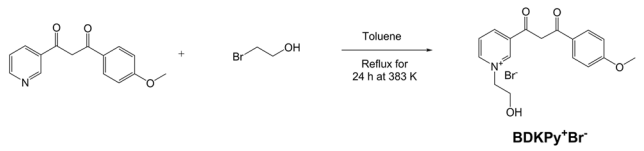

Scheme 3 Synthesis of $BDKPy^+Br^-$ *via* the quaternization of BDK.

resulting organic supernatant was performed by evaporation under reduced pressure, which produced a crystallized powder of 1-(4-methoxyphenyl)-3-(pyridine-3-yl)-propane-1,3-dione (abbreviated as BDK).

The quaternization of BDK (Scheme 3) was conducted by refluxing a mixture of 2-bromoethanol (0.26 g, 2 mmol) with BDK (0.26 g, 1 mmol) dissolved in 10 mL of dry toluene at 383 K for 24 h. After cooling to room temperature, the filtered solid was washed with toluene to remove unreacted BDK and 2-bromoethanol to obtain $BDKPy^+Br^-$ as a powder (0.34 g, 0.89 mmol) in 90% yield. The structure of $BDKPy^+Br^-$ was analyzed by ^1H nuclear magnetic resonance (NMR; see the ESI, Fig. S1†) and mass spectrometry (MS; Fig. S2†). ^1H NMR (400 MHz, DMSO-d_6): 9.70 (s, 1H, Py H), 9.25 (d, J = 8.3 Hz, 1H, Py H), 9.17 (d, J = 6.0 Hz, 1H, Py H), 8.35 (dd, J = 8.1 and 6.1 Hz, 1H, Py H), 8.25 (d, J = 8.9 Hz, 2H, Ar H), 7.55 (s, 1H, enol CH), 7.17 (d, J = 8.9 Hz, 2H, Ar H), 5.28 (t, 1H, OH), 4.80 (t, 2H, Ar H), 3.94 (t, 2H, Ar H), and 3.90 (s, 3H, $-OCH_3$).[43] MS (m/z): $[M + H]^+$ calcd for $C_{17}H_{19}NO_4^+$, 301.13; determined, 301.20.

Cation-exchange reactions of SA with $BDKPy^+$

After the dissolution of $BDKPy^+Br^-$ in a mixed solvent of water and ethanol (9 : 1 in volume), 0.1 g of SA was allowed to react under magnetic stirring at room temperature for 24 h. The resulting solid was recovered by filtration (Omnipore 0.1 μm polytetrafluoroethylene membrane) and dried at room temperature. Hereafter, dried solids are designated as $BDKPy^+$-Sn (n = 0.05, 0.1, 0.2, 0.3, 0.5, and 1), in which the amount of $BDKPy^+Br^-$ added to the solution was 0.05, 0.1, 0.2, 0.3, and 0.5 times the CEC of SA, respectively, in addition to the amount equivalent to CEC. The volume of solvent varied in the range of 5.9 mL to 118 mL, whereas the concentration of the $BDKPy^+Br^-$ solution remained constant (6.0 mM). The amount of adsorbed $BDKPy^+Br^-$ on SA was determined from the change in the concentration of the supernatant before and after adsorption using a visible absorption spectrophotometer (λ_{abs} = 365 nm).

Co-adsorption of photo-inactive species

After 0.1 g of SA was mixed with a 6.0 mM $BDKPy^+Br^-$ solution (11.8 mL; the amount of included $BDKPy^+Br^-$ was equivalent to 0.1 CEC) under magnetic stirring at room temperature, PVP was immediately added to the mixture and allowed to react for 24 h. The amount of added PVP varied from 1 mg to 100 mg relative to that (0.1 g) of SA. The resulting solid was collected using filtration and subsequent drying at room temperature. Hereafter, dried solids are designated as $BDKPy^+$-S0.1-PVPm (m = 0.01, 0.10, 0.15, 0.25, 0.5, and 1.0) according to the mass ratio of PVP to SA.

Instead of PVP, cationic species (TMA^+Cl^- and BA–HCl) were also used by changing the amount toward that of pre-adsorbed $BDKPy^+$ on SA. Particularly, a mixture was prepared, which contained 0.1 g of SA and a 6.0 mM $BDKPy^+Br^-$ solution with an appropriate volume (in the range of 11.8–59.0 mL, in which the amount of included $BDKPy^+Br^-$ was in the range of 0.1–0.5 CEC, respectively), and then TMA^+Cl^- or BA–HCl were added to the mixture in the range of 0.1–0.5 CEC. After magnetic stirring at room temperature for 24 h, centrifugation and the subsequent drying of the precipitate at room temperature produced powder samples. Dried solids are designated as $BDKPy^+$-Sn-TMAx and $BDKPy^+$-Sn-BAx (n and x = 0.1, 0.2, 0.3, 0.4, and 0.5).

Equipment

^1H NMR (400 MHz) spectra were recorded using a JEOL JNM-EX400 spectrometer in deuterated dimethyl sulfoxide (DMSO). Mass spectra were recorded using a Bruker Autoflex Speed spectrometer. UV–Vis spectra were recorded on a Shimadzu UV–2450PC spectrophotometer. Steady-state fluorescence spectra were recorded using a Shimadzu RF-5300PC fluorescence spectrophotometer. Quantum yield measurements (solid state and solution) were performed using a Hamamatsu photonics C9920-02 instrument. XRD patterns were obtained using a Rigaku RINT 2200 V/PC diffractometer (monochromatic Cu Kα radiation) operated at 20 mA and 40 kV. Fluorescence decay profiles were measured using the time-correlated single-photon counting (TCSPC) technique. A picosecond light pulse with the wavelength of 375 nm (LDB-160C, Tama Electric Inc.) was used as the excitation light source. Fluorescence from samples was passed through a visible band-pass filter (center wavelength of 500 ± 2 nm, FWHM = 10 ± 2 nm, FB500-10, Thorlabs) and detected with an avalanche photodiode (SPD-050-CTE, Micro Photon Device). TCSPC traces were recorded with a counting board (SPC-130, Becker & Hickl GmbH).

3. Results and discussion

Cation-exchange reactions of SA with $BDKPy^+Br^-$

The adsorbed amount of $BDKPy^+$ on SA from an aqueous solution is summarized in Table 1. Owing to strong electrostatic interactions between $BDKPy^+$ and anionic silicate layers of SA, all $BDKPy^+$ applied to SA adsorbed on SA within the CEC (0.71 mEq g^{-1} SA). The XRD patterns of the resulting solids ($BDKPy^+$-Sn) are shown on the left side of Fig. 1 together with that of pristine SA. A poor crystallinity of SA yielded to a low intensity of diffraction. The expansion of the interlayer space of SA by $BDKPy^+$ (intercalation) was confirmed by the shifting of the (001) diffraction peak to a lower 2θ region with an increase in the amount of $BDKPy^+$. The basal spacing of pristine SA (1.23 nm) slightly increased to the values listed in

Table 1 List of the adsorbed amount of $BDKPy^+$ on SA, basal spacing, and optical properties

	Adsorbed amount [mEq g^{-1}]	Basal spacing [nm]	λ_{em} [a] [nm]	Quantum yield [c] [%]
Solution	—	—	n.d. [b]	0.4
$BDKPy^+$-S0.05	0.035	1.32	491	38 (—)
$BDKPy^+$-S0.1	0.070	1.33	495	40 (47)
$BDKPy^+$-S0.2	0.14	1.33	492	32 (50)
$BDKPy^+$-S0.3	0.21	1.35	492	19 (47)
$BDKPy^+$-S0.5	0.35	1.36	499	10 (7.4)
$BDKPy^+$-S1	0.68	1.39	500	4.4 (—)

[a] Photoluminescence maximum (excited at 365 nm). [b] The luminescence was extremely weak. [c] Measured as powder for intercalation compounds; the value in parentheses designates a dispersion in a water/ethanol mixture of 9 : 1 = v/v.

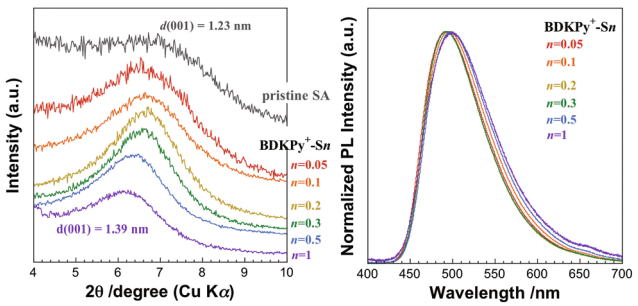

Fig. 1 XRD patterns of $BDKPy^+$-S*n* and pristine SA (left), and the normalized photoluminescence (λ_{ex} = 365 nm) spectra of $BDKPy^+$-S*n* (right).

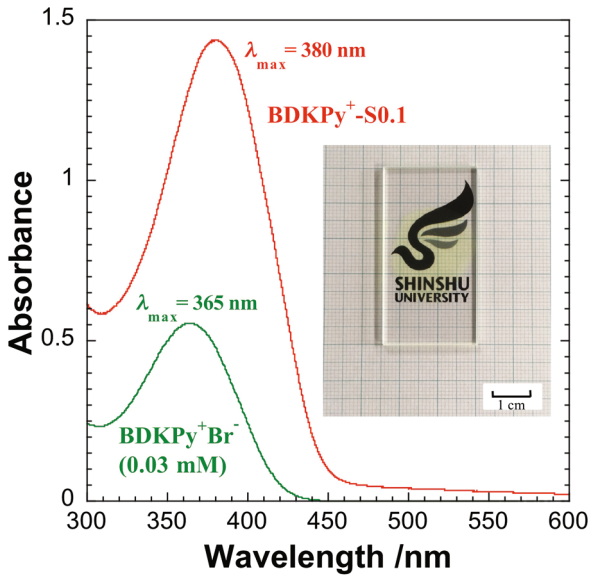

Fig. 2 Absorption spectra of an aqueous solution of $BDKPy^+Br^-$ (0.03 mM; ε = 2.0 × 10^4 mol^{-1} L cm^{-1}) and the $BDKPy^+$-S0.1 cast film that was prepared by depositing a dispersion on a quartz plate (photograph).

Table 1 and finally to 1.39 nm for the $BDKPy^+$-S1 sample. The interlayer space determined by subtracting the thickness of silicate layer (0.96 nm) from the observed basal spacing was 0.4 nm. This value was in agreement with the size of methylene groups, which indicated the monomolecular coverage of adsorbed $BDKPy^+$ with their molecular plane parallel to the silicate layer.

A transparent supported film was obtained by depositing the dispersion ($BDKPy^+$-S0.1) on a quartz substrate, as shown in Fig. 2. The absorption band maximum (at 380 nm) in the spectrum was located in the longer wavelength region compared with that of the dilute solution (0.03 mM) of $BDKPy^+Br^-$ (at 365 nm). Owing to its large dipole in the ground state, the position of the maximum in solution shifted to a longer wavelength with a decrease in solvent polarity (the absorption spectra in water, methanol, acetonitrile, tetrahydrofuran, and chloroform are shown in the ESI, Fig. S3†) and was in the range of 365–385 nm. In addition, a variation in solvent polarity affected the absorption maximum for interlayer $BDKPy^+$ in SA silicate layers, which was in the range of 370–400 nm (the absorption spectra of $BDKPy^+$-S0.1 in various solvents are shown in the ESI, Fig. S4†). Thus, the bathochromic shift observed for $BDKPy^+$-S0.1 was presumably attributed to a change in the π orbital of $BDKPy^+$ by approaching the negatively charged oxygen 6-membering ring of the siloxane surface of SA in the ground state. Regardless of the variation in the adsorbed amount of $BDKPy^+$, the position of the absorption maximum did not change (Fig. S5 in the ESI†).

The normalized photoluminescence spectra of $BDKPy^+$-S*n* are shown on the right side of Fig. 1. The photoluminescence maximum λ_{em} was located at approximately 500 nm (Table 1). When $BDKPy^+Br^-$ was dissolved in solvents (*e.g.*, water, methanol, acetonitrile, tetrahydrofuran, and chloroform), the location of λ_{em} at approximately 500 nm did not change, irrespective of the solvents used (the photoluminescence spectra are shown in the ESI, Fig. S6†). This means that the dipole in solutions became small in the excited state. As shown in Fig. 3, a strong bluish-green emission emerged immediately after the immersion of the SA powder into the solution of $BDKPy^+Br^-$ under UV light irradiation; whereas negligible emission was observed for the water/ethanol (9 : 1) solution (the photoluminescence spectrum is shown in the ESI, Fig. S7†). The enhanced emission induced by SA was represented by the fluorescence quantum yield (ϕ_f) in the solid state (in the range of 0.044–0.40), which was considerably different from that (<0.01) for $BDKPy^+Br^-$ in solution (Table 1). The ϕ_f value saturated when the amount of adsorbed $BDKPy^+$

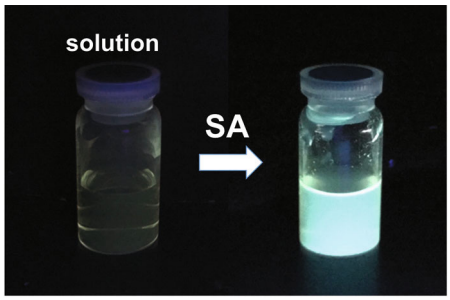

Fig. 3 Photograph of a 0.6 mM solution of $BDKPy^{+}Br^{-}$ (left) and the mixture with SA (right).

was 0.070 mmol g^{-1} ($BDKPy^{+}$-S0.1), whereas concentration quenching occurred at the high loading of $BDKPy^{+}$ on SA, which resulted in a decrease in ϕ_f. The result of equivalent ϕ_f (0.47 for $BDKPy^{+}$-S0.1) to the powder sample (ϕ_f = 0.40) showed that solvent molecules in the dispersion did not cause quenching of the excited state. The time-resolved fluorescence spectrum measurement of $BDKPy^{+}$-S0.1 in solution afforded a decay curve that could be fitted to a single exponential decay (the excitation lifetime τ_f was determined to be 2.2 ns in λ_{em} = 500 ± 2 nm).

High luminescence efficiency indicates restricted intramolecular motion (*e.g.*, rotation and vibration), which can be dictated by a non-radiative deactivation rate constant for fluorescence (k_{nr}) given by ϕ_f (0.47) and τ_f (2.2 ns), according to eqn (1).[44]

$$k_{nr} = (1 - \phi_f)/\tau_f \quad (1)$$

The calculated k_{nr} value was 0.23 × 10^9 s^{-1}. This value should be smaller, considering the smaller ϕ_f value of 0.0040 in the solution (the excitation lifetime was not measured owing to extremely weak emission). The crucial role of nanosheets in dye binding has been demonstrated as "surface-fixation induced emission (S-FIE)",[3] as has been proposed by Takagi *et al.* They have reported emission enhancement of various cations by SA nanosheets on the basis of the k_{nr} value and ϕ_f ratio with/without SA (Table 2). The suppression of non-radiative deactivation has been explained in terms of the restriction of vibrational motion using a planar dye on flat silicates without aggregation.[4,36,37]

Table 2 summarizes the photoluminescence efficiency for the $BDKPy^{+}$ system on the basis of the k_{nr} value and ϕ_f ratio with/without SA. Because these values are comparable to those reported for polyvalent cation systems, the silicate layers of SA also participate in suppressing the intramolecular vibrational motion of $BDKPy^{+}$, which was confined in narrow two-dimensional nanospaces (the interlayer distance of 0.4 nm) in dispersion. However, as described above, a dense packing (n > 0.2) resulted in the degradation of luminescence efficiency (ϕ_f). The threshold of packing density presumably allowed to enhance emission, according to the literature on primary pyridinium diketonate-incorporated layered silicate (SA).[28]

Co-adsorption of photo-inactive species

We focused on the basal spacing (interlayer space) and packing density of $BDKPy^{+}$ in SA. First, we will discuss the effect of the interlayer space (distance) on luminescence efficiency; therefore, the co-adsorption of a water-soluble polymer (PVP)[40] was employed to consider the interlayer expansion. We prepared samples, which included $BDKPy^{+}$ in an amount that was equivalent to that of the PVP-free sample ($BDKPy^{+}$-S0.1). Table 3 shows the basal spacing of the powder products and the photochemical properties (λ_{em}, τ_f, ϕ_f, k_f, and k_{nr}) of their dispersions. A gradual increase in the basal spacing is indicative of the intercalation in response to the applied amount of PVP. When the amount of PVP was increased up to 0.25 *versus* 1 g of SA, the fluorescence quantum yield ϕ_f was approximately 50%. The intramolecular motion is also restricted when the PVP amount is less than 0.25, judging from the comparable values of k_{nr} to that of the PVP-free sample (0.23). However, above 0.5 g of PVP, the quantum yield ϕ_f dropped, and the k_{nr} value increased. Fig. 4 shows the relationship between the interlayer space with the fluorescence quantum yield ϕ_f (Fig. 4a) and the non-radiative deactivation rate constant k_{nr} for fluorescence (Fig. 4b). Considering an increase in the interlayer distance from 1.05 nm to 1.88 nm (an increase in the basal spacing from 2.01 nm to 2.84 nm), the restricted intramolecular motion will be relaxed by the interlayer expansion. A spectral blue shift in

Table 2 Comparison of photoluminescence efficiency enhanced by SA depending on adsorbed cations

Cations	State	Surface density of cation[a] [×10^{-2} nm^{-2}]	k_{nr} [×10^9 s^{-1}]	ϕ_f ratio on SA/in solution	Ref.
$BDKPy^{+}$ (10% CEC)	Dispersion in water/EtOH (90%)	6	0.23	1.2 × 10^2	This study
$BDKPy^{+}$ (10% CEC) + 0.15 g PVP per g	Dispersion in water/EtOH (90%)	6	0.15	1.3 × 10^2	This study
$BDKPy^{+}$ (50% CEC) + TMA (50% CEC)	Dispersion in water/EtOH (90%)	30	0.35	83	This study
BDK^{+} (primary)	Powder[b]	10	1.0	1 × 10^3	28
$Porphyrazine^{4+}$	Dispersion in water	0.1	0.24 (stacked)	19	4
			0.90 (exfoliated)	10	
Boron $subporphyrin^{3+}$	Dispersion in water	0.06	0.04	1.3	37
p-Substituted $triphenylbenzene^{3+}$	Dispersion in water	3	0.19	5.5	36

[a] Calculated by dividing the amount of cations on SA by the ideal surface area of SA (690 m^2 g^{-1}), when measuring the excitation lifetime. [b] Dispersion in water was non-emissive.

Table 3 List of basal spacing (interlayer distance) and optical properties in the presence of PVP

	Basal spacing [nm]	λ_{em} [a] [nm]	ϕ_f [b] [%]	τ_f [b] [ns]	k_{nr} [ns^{-1}]	k_f [c] [ns^{-1}]
$BDKPy^+$-S0.1	1.33 (0.37)	495	47	2.2	0.23	0.21
$BDKPy^+$-S0.1-PVP0.01	1.34 (0.38)	495	52	2.9	0.17	0.18
$BDKPy^+$-S0.1-PVP0.10	1.52 (0.56)	495	50	2.9	0.17	0.17
$BDKPy^+$-S0.1-PVP0.15	1.63 (0.67)	495	53	3.1	0.15	0.17
$BDKPy^+$-S0.1-PVP0.25	2.01 (1.05)	495	49	2.2	0.23	0.22
$BDKPy^+$-S0.1-PVP0.50	2.57 (1.61)	485	32	2.4	0.29	0.13
$BDKPy^+$-S0.1-PVP1.0	2.84 (1.88)	485	18	2.7	0.30	0.066
$BDKPy^+$-S0.1-TMA0.1	1.33 (0.37)	487	57	2.5	0.17	0.23
$BDKPy^+$-S0.1-BA0.1	1.36 (0.40)	485	59	3.3	0.12	0.18
$BDKPy^+$-S0.2	1.33 (0.37)	492	50	3.1	0.16	0.16
$BDKPy^+$-S0.2-TMA0.2	1.40 (0.44)	486	48	3.0	0.17	0.23
$BDKPy^+$-S0.2-BA0.2	1.32 (0.36)	485	43	3.0	0.19	0.14
$BDKPy^+$-S0.3	1.35 (0.39)	492	47	3.1	0.17	0.15
$BDKPy^+$-S0.3-TMA0.3	1.36 (0.40)	486	37	2.1	0.29	0.17
$BDKPy^+$-S0.3-BA0.3	1.35 (0.39)	485, 540	29	2.8	0.26	0.10
$BDKPy^+$-S0.5	1.36 (0.40)	499	7.4	1.7	0.56	0.028
$BDKPy^+$-S0.5-TMA0.5	1.38 (0.42)	488	33	1.9	0.35	0.17
$BDKPy^+$-S0.5-BA0.5	1.35 (0.39)	485, 540	14	2.1	0.41	0.066

[a] Photoluminescence maximum (excited at 365 nm). [b] Measured as a dispersion in a water/ethanol mixture of 9 : 1 = v/v, and all decay curves can be analysed as a single exponential decay. [c] Radiative deactivation rate constant for fluorescence k_f, according to eqn $k_f = (1/\tau_f) - k_{nr}$.

the absorption spectra (Fig. S8 in ESI†) is attributed to the environmental change of $BDKPy^+$ surrounded by intercalated PVP.

Conversely, some photo-inactive cations (TMA^+ and BA^+) were examined for co-adsorption because these cations are expected to be suitable to preserve a narrow interlayer distance for the tight binding of $BDKPy^+$. When TMA^+ or BA^+ was co-adsorbed, each product included $BDKPy^+$ as an equivalent amount in $BDKPy^+$-S*n* samples, as confirmed by UV–vis analyses. The basal spacings were approximately 1.4 nm for $BDKPy^+$-S*n*-TMA*x* and $BDKPy^+$-S*n*-BA*x* (x = 0.1, 0.2, 0.3, and 0.5), which corresponded to the interlayer distance/space of 0.4 nm (Table 3). Plots were added in Fig. 4 to show the relationship of the interlayer space with ϕ_f (Fig. 4a) and with k_{nr} (Fig. 4b). The ϕ_f value became high and saturated at approximately 60% when the amount of adsorbed $BDKPy^+$ was 0.070 mmol g^{-1} ($BDKPy^+$-S0.1-TMA0.1 and -BA0.1). The co-adsorption of BA^+ enhanced concentration quenching owing to the remarkable diminishing ϕ_f and k_f with an increase in the loaded amounts of $BDKPy^+$ and BA^+. In addition, a new band in the normalized photoluminescence spectrum appeared at 540 nm (Fig. 5a), which indicated the aggregation of $BDKPy^+$ on SA, which was similar to an intraparticle phase separation in the nanospace between $BDKPy^+$ and BA^+ (Scheme 4a). However, TMA^+ cations were determined to contribute to the reduction of concentration quenching because ϕ_f (33%) of $BDKPy^+$-S0.5-TMA0.5 was much higher than that (7.4%) without TMA^+. A lack of emission owing to $BDKPy^+$ aggregates (λ_{em} = 540 nm) was illustrated by the normalized photoluminescence spectra (Fig. 5b). Therefore, the molecular isolation of proximal $BDKPy^+$ can be achieved by the co-insertion of TMA^+ in the interlayer space (Scheme 4b).

The higher loading of luminogens is important for producing highly emissive solids for various applications. Table 2 summarizes the relationship between photoluminescence efficiency and surface density of luminogenic cations. Cation-exchangeable layered silicates, including smectites, are useful supports for cationic luminogens owing to the large CEC. However, in general, limited control of adsorbed luminogenic cations was frequently observed owing to their aggregation; thus, molecular design was utilized. The reported polyvalent

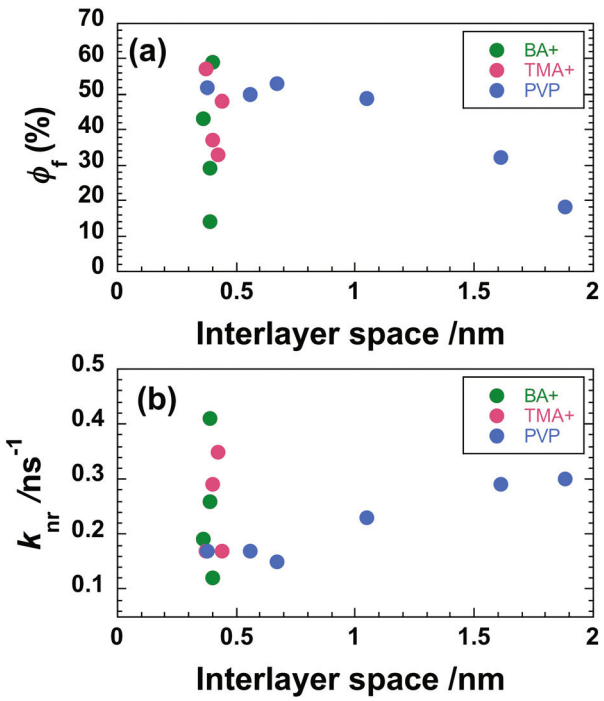

Fig. 4 Relationship between the interlayer space with (a) fluorescence quantum yield ϕ_f and (b) non-radiative deactivation rate constant k_{nr} for fluorescence.

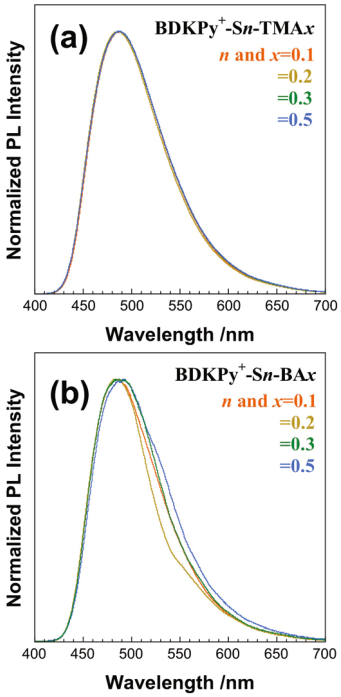

Fig. 5 Photoluminescence (λ_{ex} = 385 nm) spectra of (a) BDKPy$^+$-S*n*-TMA-*x* and (b) BDKPy$^+$-S*n*-BA-*x* (*n* and *x* = 0.1, 0.2, 0.3, and 0.5) in a water/ethanol (9 : 1) mixture.

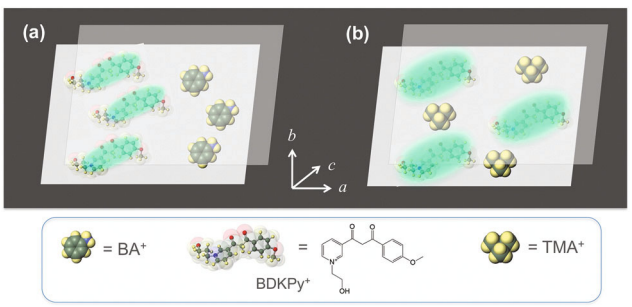

Scheme 4 Schematic drawing of the possible interlayer structures of (a) BDKPy$^+$-S0.5-BA-0.5 and (b) BDKPy$^+$-S0.5-TMA-0.5.

cationic dyes shown in Table 2 are good examples of how to prevent aggregation to exhibit the "S-FIE" phenomenon[4,36,37] when positive charges on cationic dyes geometrically match a negative layer charge on layered silicate.[31] Although the described BDKPY is a monovalent cation that tends to produce dense packing, concentration quenching can be prevented by the co-adsorption of a small aliphatic cation, TMA. The intercalation of TMA has been frequently used as a pillaring agent to produce microporous solids with pore sizes of approximately 0.5 nm.[33,39,45–47] It can be observed that the co-adsorption of cations is an artificial energy transfer system with a controlled spatial distribution of energy donors/acceptors.

4. Conclusions

Layered silicate (SA) was determined to be an excellent support for quaternary pyridyl-β-diketonate (BDKPy$^+$) to achieve enhanced emission. This is achieved by avoiding concentration quenching and by suppressing the intramolecular motion in the interlayer space with the aid of electrostatic dye–silicate interactions. The restriction of intramolecular motion of BDKPy$^+$ was confirmed by a smaller non-radiative deactivation rate constant k_{nr} for green fluorescence with a quantum yield ϕ_f and fluorescence lifetime τ_f. Basal spacing (interlayer space) was responsible for the restricted motion. With an increase in the interlayer space above 1.0 nm by co-adsorbing PVP, the quantum yield ϕ_f decreased, and the non-radiative deactivation rate constant k_{nr} eventually increased. When the loaded amount of BDKPy$^+$ was varied, the quantum yield ϕ_f saturated at 10% CEC (an adsorbed BDKPy$^+$ amount of 0.07 mmol g^{-1} of SA). This was indicative of the moderate distance between adjacent BDKPy$^+$ cations. The co-adsorption of photo-inactive TMA$^+$ cations was determined to be effective for avoiding concentration quenching because a higher quantum yield ϕ_f (33%) was obtained compared to that in the absence of TMA$^+$ (7.4%) even at the higher loading level of BDKPy$^+$: 0.35 mmol g^{-1} of SA, 0.3 nm^{-2} of (SA). The interlayer space was maintained within 0.4 nm, which suppressed the intramolecular motion of BDKPy$^+$ by binding silicate layers.

The high loading (dense packing) of luminophores is advantageous for light emitting applications and photo-induced energy transfer reactions (*e.g.*, light harvesting). Upon the deactivation of the excited energy of a luminophore by a proximal energy acceptor, the spatial distribution of donors and acceptors should be important for light harvesting systems.[48] If the photo-inactive species described in this study are replaced with an appropriate energy acceptor, the obtained results suggest ways of creating efficient artificial energy transfer systems, in which the luminescence efficiency depends on the selected adsorbed species.

Conflicts of interest

There are no conflicts to declare.

Acknowledgements

This work was supported by JSPS KAKENHI (Grant-in-Aid for Scientific Research), grant numbers of 26810121, 20K05661 (T. O.), 26410009, JP15H01081, JP17H05253, and JP19H02686 in Scientific Research on Innovative Areas "Photosynergetics" (F. I.). Mukai Science and Technology Foundation also supported us (T. O.) financially. We acknowledge Professor Tsuyoshi Fukaminato (Kumamoto University) for measurement of mass spectrometry and Dr Minoru Sohmiya (Waseda University) for measurement of fluorescence quantum yield.

Notes and references

1 J. Mei, N. L. C. Leung, R. T. K. Kwok, J. W. Y. Lam and B. Z. Tang, Aggregation-Induced Emission: Together We Shine, United We Soar!, *Chem. Rev.*, 2015, **115**, 11718–11940.

2 J. Mei, Y. Hong, J. W. Y. Lam, A. Qin, Y. Tang and B. Z. Tang, Aggregation-Induced Emission: The Whole Is More Brilliant than the Parts, *Adv. Mater.*, 2014, **26**, 5429–5479.

3 D. Tokieda, T. Tsukamoto, Y. Ishida, H. Ichihara, T. Shimada and S. Takagi, Unique Fluorescence Behavior of Dyes on the Clay Minerals Surface: Surface Fixation Induced Emission (S-FIE), *J. Photochem. Photobiol., A*, 2017, **339**, 67–79.

4 Y. Ishida, T. Shimada and S. Takagi, "Surface-Fixation Induced Emission" of Porphyrazine Dye by a Comlexation with Inorganic Nanosheets, *J. Phys. Chem. C*, 2014, **118**, 20466–20471.

5 R. Nakazato, K. Sano, H. Ichihara, T. Ishida, T. Shimada and S. Takagi, Factors for the Emission Enhancement of Dimidium in Specific Media Such as in DNA and on a Clay Surface, *Phys. Chem. Chem. Phys.*, 2019, **21**, 22732–22739.

6 G. F. de Sá, O. L. Malta, C. de Mello Donegá, A. M. Simas, R. L. Longo, P. A. Santa-Cruz and E. F. da Silva Jr., Spectroscopic Properties and Design of Highly Luminescent Lanthanide Coordination Complexes, *Coord. Chem. Rev.*, 2000, **196**, 165–195.

7 Y. Hasegawa, Y. Wada and S. Yanagida, Strategies of the Design of Luminescent Lanthanide (III) Complexes and Their Photonic Applications, *J. Photochem. Photobiol., C*, 2004, **5**, 183–202.

8 G. Zhang, S. H. Kim, R. E. Evans, B. H. Kim, J. N. Demas and C. L. Luminescent, Donor-Acceptor Beta-Diketones: Modulation of Emission by Solvent Polarity and Group II Metal Binding, *J. Fluoresc.*, 2009, **19**, 881–889.

9 A. Kuno, M. Fujiwara, Y. Haketa and H. Maeda, Arylpyrrolyldiketone Boron Complexes Exhibiting Various Anion-Binding Modes Based on Dynamic Conformation Changes, *Chem. – Asian J.*, 2019, **14**, 1777–1785.

10 H. Kita, R. Yamamoto, R. Fukuuchi, T. Konishi, K. Kamada, Y. Haketa and H. Maeda, Switching of Two-Photon Optical Properties by Anion Binding of Pyrrole-Based Boron Diketonates through Conformation Change, *Chem. – Eur. J.*, 2020, **26**, 3404–3410.

11 M. Tsuchikawa, A. Takao, T. Funaki, H. Sugihara and K. Ono, Multifunctional Organic Dyes: Anion-Sensing and Light-Harvesting Properties of Curcumin Boron Complexes, *RSC Adv.*, 2017, **7**, 36612–36616.

12 B. L. Tang, H. Zhang, C. Cheng, K. Ye and H. Zhang, 1,3-Diaryl-*β*-diketone Organic Crystals with Red Amplified Spontaneous Emission, *ChemPlusChem*, 2016, **81**, 1320–1325.

13 A. Nagai, K. Kokado, Y. Nagata, M. Arita and Y. Chujo, Highly Intense Fluorescent Diarylboron Diketonate, *J. Org. Chem.*, 2008, **73**, 8605–8607.

14 G. Zhang, J. Lu, M. Sabat and C. L. Fraser, Polymorphism and Reversible Mechanochromic Luminescence for Solid-State Difluoroboron Avobenzone, *J. Am. Chem. Soc.*, 2010, **132**, 2160–2162.

15 G. Zhang, R. E. Evans, K. A. Campbell and C. L. Fraser, Role of Boron in the Polymer Chemistry and Photophysical Properties of Difluoroboron-Dibenzoylmethane Polylactide, *Macromolecules*, 2009, **42**, 8627–8633.

16 G. Zhang, J. P. Singer, S. E. Kooi, R. E. Evans, E. L. Thomas and C. L. Fraser, Reversible Solid-State Mechanochromic Fluorescence from a Boron Lipid Dye, *J. Mater. Chem.*, 2011, **21**, 8295–8299.

17 T. Butler, W. A. Morris, J. Samonina-Kosicka and C. L. Fraser, Mechanochromic Luminescence and Aggregation Induced Emission for a Metal-Free *β*-Diketone, *Chem. Commun.*, 2015, **51**, 3359–3362.

18 F. Ito, Y. Suzuki, J. Fujimori, T. Sagawa, M. Hara, T. Seki, R. Yasukuni and M. L. Chapelle, Direct Visualization of the Two-step Nucleation Model by Fluorescence Color Changes during Evaporative Crystallization from Solution, *Sci. Rep.*, 2016, **6**, 22918.

19 H.-W. Mo, Y. Tsuchiya, Y. Geng, T. Sagawa, H. Nakanotani, F. Ito and C. Adachi, Color Tuning of Avobenzone Boron Difluoride as an Emitter to Achieve Full-Color Emission, *Adv. Funct. Mater.*, 2016, **26**, 6703–6710.

20 F. Ito and C. Kikuchi, Concentration-Dependent Fluorescence Color Tuning of the Difluoroboron Avobenzone Complex in Polymer Films, *Bull. Chem. Soc. Jpn.*, 2017, **90**, 709–713.

21 T. Butler, W. A. Morris, J. Samonina-Kosicka and C. L. Fraser, Mechanochromic Luminescence and Aggregation Induced Emission of Dinaphtoylmethane *β*-Diketones and Their Boronated Counterparts, *ACS Appl. Mater. Interfaces*, 2016, **8**, 1242–1251.

22 T. Butler, M. A. Zhuang and C. L. Fraser, Tuning of Mechanochromic Luminescent *β*-Diketones via Boron Coordination and Donor-Acceptor Effects, *J. Phys. Chem. C*, 2018, **122**, 19090–19099.

23 J. Feng and H. Zhang, Hybrid Materials Based on Lanthanide Organic Complexes: A Review, *Chem. Soc. Rev.*, 2013, **42**, 387–410.

24 C. Sanchez, B. Lebeau, F. Chaput and J.-P. Boilot, Optical Properties of Functional Hybrid Organic-Inorganic Nanocomposites, *Adv. Mater.*, 2003, **15**, 1969–1994.

25 K. Binnemans, Lanthanide-Based Luminescent Hybrid Materials, *Chem. Rev.*, 2009, **109**, 4283–4374.

26 V. Divya and L. P. Reddy, Visible-Light Excited Red Emitting Luminescent Nanocomposites Derived from Eu^{3+}-Phenathrene-Based Fluorinated β-Diketonate Complexes and Multi-Walled Carbon Nanotubes, *J. Mater. Chem. C*, 2013, **1**, 160–170.

27 K. Kuriki, Y. Koike and Y. Okamoto, Plastic Optical Fiber Lasers and Amplifiers Containing Lanthanide Complexes, *Chem. Soc. Rev.*, 2002, **102**, 2347–2356.

28 M. Hirose, F. Ito, T. Shimada, S. Takagi, R. Sasai and T. Okada, Photoluminescence by Intercalation of a

Fluorescent β-Diketone Dye into a Layered Silicate, *Langmuir*, 2017, **33**, 13515–13521.
29 M. Ogawa and K. Kuroda, Photofunctions of Intercalation Compounds, *Chem. Rev.*, 1995, **95**, 399–438.
30 T. Okada, Y. Ide and M. Ogawa, Organic-Inorganic Hybrids Based on Ultrathin Oxide Layers –Designed Nanostructures for Molecular Recognition, *Chem. – Asian J.*, 2012, **7**, 1980–1992.
31 S. Takagi, T. Shimada, Y. Ishida, T. Fujimura, D. Masui, H. Tachibana, M. Eguchi and H. Inoue, Size-Matching Effect on Inorganic Nanosheets: Control of Distance, Alignment, and Orientation of Molecular Adsorption as a Bottom-Up Methodology for Nanomaterials, *Langmuir*, 2013, **29**, 2108–2119.
32 T. Okada, M. Sohmiya and M. Ogawa, Photochromic Intercalation Compounds, *Struct. Bonding*, 2015, **166**, 177–211.
33 T. Okada and M. Ogawa, Inorganic–Organic Interactions, in *Inorganic Nanosheets and Nanosheet-Based Materials*, ed. T. Nakato, J. Kawamata and S. Takagi, Springer Japan KK, Tokyo, 2017, ch. 6, pp. 163–186.
34 G. Villemure, C. Detellier and A. Z. Szabo, Fluorescence of Clay-Intercalated Methylviologen, *J. Am. Chem. Soc.*, 1986, **108**, 4658–4659.
35 G. Villemure, C. Detellier and A. Z. Szabo, Fluorescence of Methylviologen Intercalated into Montmorillonite and Hectorite Aqueous Suspensions, *Langmuir*, 1991, **7**, 1215–1221.
36 T. Tsukamoto, T. Shimada and S. Takagi, Unique Photochemical Properties of *p*-Substituted Cationic Triphenylbenzene Derivatives on a Clay Layer Surface, *J. Phys. Chem. C*, 2013, **117**, 2774–2779.
37 T. Tsukamoto, T. Shimada and S. Takagi, Photophysical Properties and Adsorption Behaviors of Novel Tri-Cationic Boron(III) Subporphyrin on Anionic Clay Surface, *ACS Appl. Mater. Interfaces*, 2016, **8**, 7522–7528.
38 M. Ogawa, M. Inagaki, N. Kodama, K. Kuroda and C. Kato, Novel Controlled Luminescence of Tris(2,2′-bipyridine) ruthenium(II) Intercalated in a Fluortetrasilicic Mica with Poly(vinylpyrrolidone), *J. Phys. Chem.*, 1993, **97**, 3819–3823.
39 M. Ogawa, M. Takahashi, C. Kato and K. Kuroda, Oriented Microporous Film of Tetramethylammonium Pillared Saponite, *J. Mater. Chem.*, 1994, **4**, 519–523.
40 M. Ogawa, M. Tsujimura and K. Kuroda, Incorporation of Tris(2,2′-bipyridine)ruthenium(II) in a Synthetic Swelling Mica with Poly(vinylpyrrolidone), *Langmuir*, 2000, **16**, 4202–4206.
41 M. Sohmiya, S. Omata and M. Ogawa, Two Dimensional Size Controlled Confinement of Poly(vinyl pyrrolidone) in the Interlayer Space of Swelling Clay Mineral, *Polym. Chem.*, 2012, **3**, 1069–1074.
42 S. Nakanishi, K. Yao, M. Kodama, Y. Imai, K. Ogino and K. Mishima, Electrokinetc Study of Synthetic Smectites by Flat Plate Streaming Potential Technique, *Langmuir*, 2002, **18**, 188–193.
43 T. Xie, B. Zhang, X. Zhang and G. Zhang, AIE-Active β-Diketones Containing Pyridiniums: Fluorogenic Binding to Cellulose and Water-Vapour-Recoverable Mechanochromic Luminescence, *Mater. Chem. Front.*, 2017, **1**, 693–697.
44 N. J. Turro, V. Ramamurthy and J. C. Scaiano, *in Modern Molecular Photochemistry of Organic Molecules*, University Science Books, Sausalito, CA, 2010.
45 R. M. Barrer, Shape-Selective Sorbents Based on Clay Minerals: A Review, *Clays Clay Miner.*, 1989, **37**, 385–395.
46 M. A. M. Lawrence, R. K. Kukkadapu and S. A. Boyd, Adsorption of Phenol and Chlorophenols from Aqueous Solution by Tetramethylammonium- and Tetramethylphosphonium-Exchanged Montmorillonite, *Appl. Clay Sci.*, 1998, **13**, 13–20.
47 T. Okada, J. Oguchi, K. Yamamoto, T. Shiono, M. Fujita and T. Iiyama, Organoclays in Water Cause Expansion That Facilitates Caffeine Adsorption, *Langmuir*, 2015, **31**, 180–187.
48 Y. Ishida, R. Kulasekharan, T. Shimada, V. Ramamurthy and S. Takagi, Supramolecular-Surface Photochemistry: Supramolecular Assembly Organized on a Clay Surface Facilitates Energy Transfer between an Encapsulated Donor and a Free Acceptor, *J. Phys. Chem. C*, 2014, **118**, 10198–10203.

